High energy ion beam irradiation on titanium substrate in a pulsed plasma device operating with methane

2009 J. Phys. D: Appl. Phys. 42 205207

(http://iopscience.iop.org/0022-3727/42/20/205207)

IOP PUBLISHING JOURNAL OF PHYSICS D: APPLIED PHYSICS

J. Phys. D: Appl. Phys. **42** (2009) 205207 (8pp) doi:10.1088/0022-3727/42/20/205207

High energy ion beam irradiation on titanium substrate in a pulsed plasma device operating with methane

H Bhuyan[1], M Favre[1], E Valderrama[1], A Henriquez[1], G Vogel[1], H Chuaqui[1], E Wyndham[1], A Cabrera[1], E Ramos-Moore[1], P A Núñez[1], H Kelly[2], D Grondona[2] and S Goyanes[2]

[1] Departamento de Física, Pontificia Universidad Católica de Chile, Casilla 306, Santiago 22, Chile
[2] Departamento de Física, Facultad de Ciencias Exactas y Naturales, Universidad de Buenos Aires, Ciudad Universitaria, Pabellon 1, 1428 Buenos Aires, Argentina

E-mail: hbhuyan@fis.puc.cl

Received 18 March 2009, in final form 24 August 2009
Published 24 September 2009
Online at stacks.iop.org/JPhysD/42/205207

Abstract

We report the investigation of high energy ion beam irradiation on titanium (Ti) substrates at room temperature using a low energy plasma focus (PF) device operating in methane gas. The surface modifications induced by the ion beam using two different anode materials, graphite and copper, are characterized using standard surface science diagnostic tools, such as x-ray diffraction, scanning electron microscopy, energy-dispersive x-ray analysis, Raman spectroscopy and Auger electron spectroscopy. It has been found that the interaction of the pulsed PF ion beams, with characteristic energy in the 15–300 keV range, with the Ti surface, results in the formation of nanocomposite carbon structures. It is observed that the resulting ion irradiated surface morphologies are different, depending on the different anode materials, under otherwise identical operational conditions. In the case of the graphite anode the interaction of PF ion beams followed by the anode vapour with the Ti surface results in the formation of gradient layers of TiC with embedded carbon nanostructures.

1. Introduction

Carbon-based nanocomposites, composed of crystalline/amorphous nanophases mixture have recently attracted increasing interest with respect to fundamental research and engineering applications, owing to their excellent mechanical and tribological properties, smooth surface, chemical inertness and good biocompatibility [1–3]. Nevertheless, weak adhesion of these nanocomposite coatings limits the expansion of their application in diverse areas. In recent years, various interlayer or gradient multilayers including Ti or TiC are commonly used to improve the adhesion of coatings to substrates. In this context, many combinations of carbides embedded in amorphous hydrogenated (a-C : H) and un-hydrogenated carbon (a-C) matrixes have been investigated, particularly the Ti + C system due to the good mechanical properties of the TiC phase [4–10]. Several methods have been developed to synthesize TiC nanocomposites, including chemical vapour deposition, magnetron sputtering, cathodic arc plasma deposition, pulsed laser deposition and ion implantation [7–13]. Recently, the process of carbon ion implantation on substrate materials has been demonstrated to be an effective method to improve the adhesion strength [14, 15]. In this case the irradiated energetic ions sputter-clean the substrate materials, get implanted onto the substrate materials as a composition gradient layer and serve as nucleation sites for successive depositions. Among the various ion sources, plasma ion sources have recently assumed importance because of their wide range of energy and intensity spectra. The plasma focus (PF) is a rich source of intense ion beams of characteristic energy up to hundreds of kiloelectronvolts [16]. PF is basically a pulsed plasma producing device that generates high temperature (∼1–2 keV) and high density (∼10^{19}–10^{20} cm^{-3}) plasma for a short duration (∼100–150 ns) by making use of self-generated magnetic fields. This device is not only a source of high density

and high temperature plasma but also a rich source of energetic ion beams. A PF device is basically a modified form of Z-pinch device having a different type of electrode configuration. It is essentially a combination of shock tube and Z-pinch [17]. PF devices operating in the few kilo joule range are characterized by a modest operational cost and allow easy modification. These particular features of PF devices, combined with the wide energy range and high characteristic flux of the emitted ions beams, together with the possibility of high frequency operation, have attracted the interest of several researchers, in view of its potential applications in different technological fields, such as surface properties modification, thin film deposition, semiconductor doping, ion-assisted coating and production of nano-compounds [18–23].

It is known that in PF discharges, anode vapours are generally emitted during the final phase of the focus formation due to the acceleration of the current sheet and also the bombardment of energetic ions and electrons on the electrode surfaces [18, 24]. If the anode tip of a PF device is replaced by any metallic insert, part of this anode material is evaporated and combined with the working gas, giving rise to hot and dense plasma jet or bubbles [25]. Hence, a combined ion-implantation–thermal treatment–coating process will be enacted on any substrate located upstream from the anode tip. The idea here is to use two kinds of anode materials, namely copper and graphite, and to investigate the effect of high energy ion beam irradiation on titanium substrates in a low energy PF device operating with methane gas. This procedure would allow the implantation effects of the pure ion beams and the combination of ion beams and anode plasma jet, to be compared. It is found that the interaction of PF ion beams with the Ti surface, using a graphite anode, results in the formation of gradient layers of TiC with embedded carbon nanostructures.

2. Experimental details

A schematic diagram of the experimental arrangements for ion irradiation along with the plasma producing system is shown in figure 1. The plasma producing system consists of a squirrel cage electrode assembly kept inside a vacuum chamber made of brass, a capacitor bank with spark gap switch and high voltage charger. The electrode assembly comprises two coaxial cylindrical copper electrodes where the bottom end of the electrode assembly is closed and separated by a 28 mm long glass insulator sleeve. On the other hand, the top end of the electrode assembly is kept open and the annular space in between the electrodes is 25 mm. The length and the outer diameter of the central electrode, which acts as the anode, are 98 mm and 24 mm, respectively. The outer electrode (cathode) is made up of six cathode rods of length 96 mm and diameter 0.8 cm uniformly spaced coaxially at a diameter of 63 mm. The PF device is powered by a capacitor bank of 9 μF, 30 kV. At 20 kV operating voltage the capacitor bank delivers a maximum current of 157 kA with 1.8 μs quarter period. The system inductance at the maximum current is around 146 nH. A resistive divider (as voltage probe), a single groove Rogowski coil (as current probe) and a BPX65 PIN

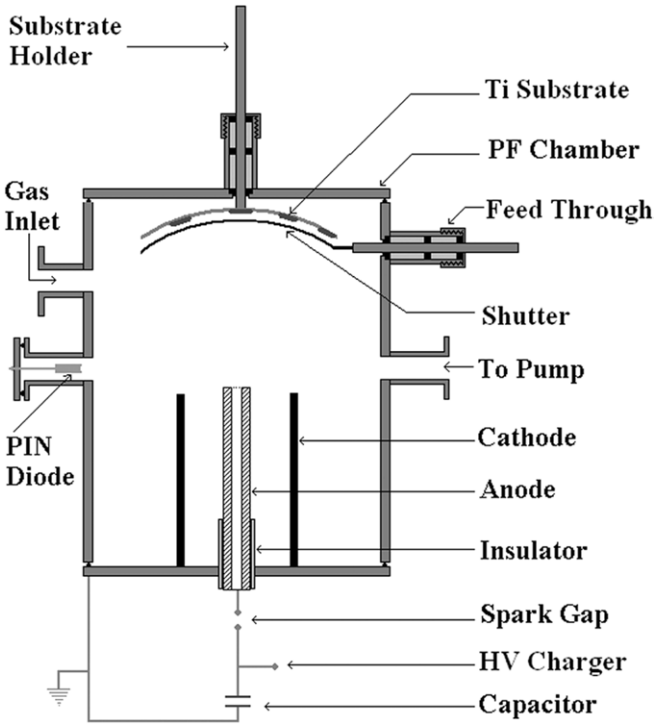

Figure 1. Experimental arrangements along with the discharge circuit.

diode (as x-ray probe) are used to ascertain the focusing action of the PF device. Further details of the PF device were reported elsewhere [24]. A surface polisher (Buehler Beta-1) is used to polish the titanium substrate before ion irradiation. These one sided mirror like polish Ti substrates were mounted at angular positions 0°, 10°, 15° and 20°, with respect to the anode axis (at a height of around 10 cm from the anode tip) using a movable substrate holder. A strong focusing action of the PF current sheets is required for the generation of high fluence energetic ion beams. This strong focusing condition is usually obtained only after a couple of conditioning PF shots. To avoid the exposure of the substrate to the weak ion beams emitted during conditioning shots, an aluminium shutter was placed in between the substrate and the ion source. The shutter was removed after the achievement of optimum operational condition, without disturbing the in vacuum conditions and thereby exposing the substrate to the energetic ions in the subsequent PF shots. The PF discharge was operated in methane gas at a pressure of around 0.3 Torr, which was found to be the optimum pressure range for focus formation at peak current, in this device [16]. Substrates were exposed to 50 successive PF discharges. In order to compare the carbon content and the resulting physio-chemical changes on the substrate surfaces, a graphite tube of 40 mm length, 24 mm outer diameter, is inserted into the open end of the anode (keeping constant the length of the anode, 98 mm). Thus the substrates were exposed in two different anode materials, namely graphite insert and copper anode with identical operating conditions. Although the graphite is an insert to the copper anode, we will refer to it as a graphite anode. The purities of the copper, titanium and graphite materials used in this experiment are 99.95%, 99.96% and

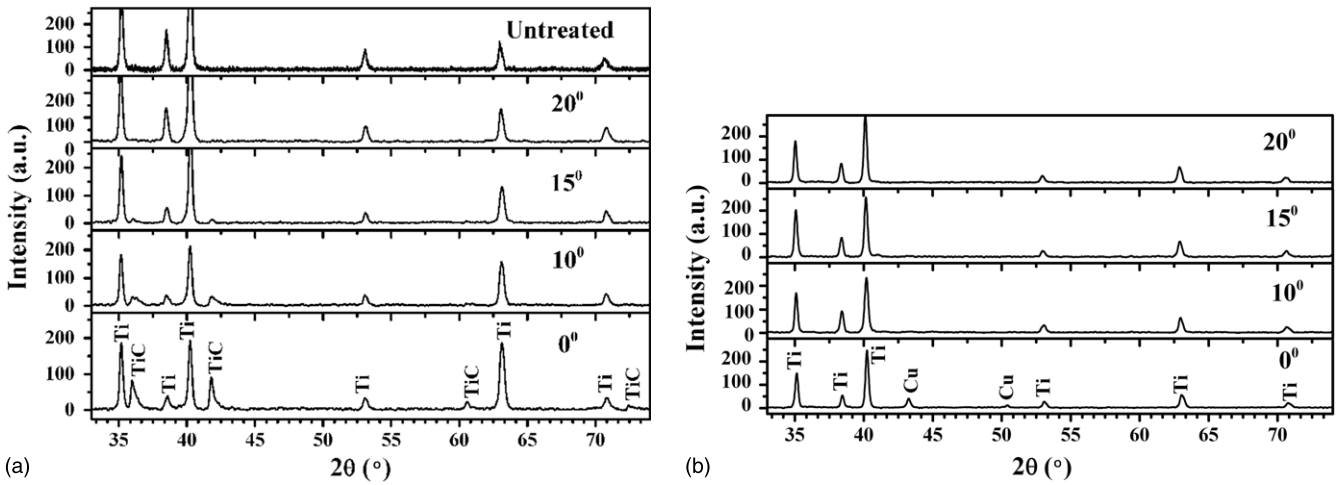

Figure 2. XRD pattern of ion exposed Ti substrates at angular positions 0°, 10°, 15° and 20° in (*a*) graphite and (*b*) copper anodes. The XRD pattern of untreated Ti substrate is shown on the top of part (*a*).

99.99%, respectively. The ion exposed substrates were later investigated by x-ray diffraction (XRD), scanning electron microscopy (SEM), energy-dispersive x-ray (EDX) analysis, Raman spectroscopy (RS) and Auger electron spectroscopy (AES). The XRD analysis was done in a D8 advance x-ray diffractometer, Bruker AXS and the diffraction data were taken from [26]. The SEM studies were performed on a LEO 1420-VP electron microscope operated at 20 kV. The EDX was performed on an Oxford Instruments INCAx-sight-7424 attached to the SEM. Unpolarized visible Raman spectra were obtained with a LabRam 010 instrument from ISA using a He–Ne laser (632.8 nm). AES analyses were performed using a DESA 100 from STAIB instruments, equipped with a double pass-cylindrical mirror analyzer and a 3 keV coaxial electron gun. The pressure in the spectrometer chamber was maintained below 1×10^{-7} Torr. The electron beam energy was 3 keV with a current of 0.4 μA and the probe area was 3×2.8 mm^2. A 5 keV Ar^+ ion beam with an ion current of 33 μA was used to obtain the depth profiles over the region 200–600 eV and are produced in the form of the dependence of $dN(E)/dE$ on E.

3. Results and discussion

The XRD patterns, θ–2θ scan mode, of ion irradiated Ti substrates at different angular positions using graphite and copper anodes are shown in figures 2(*a*) and (*b*), respectively. As shown in figure 2(*a*) the XRD pattern of ion exposed Ti substrates using a graphite anode exhibit characteristic peaks of TiC at $2\theta = 35.98°$, 41.80°, 60.60° and 72.44°, which are attributed to diffraction of cubic TiC (1 1 1), (2 0 0), (2 2 0) and (3 1 1) planes, respectively. The respective positions and relative intensities of all TiC diffraction peaks are in agreement with the standard data [26]. These patterns show the successful growth of nano- crystalline TiC on the ion exposed Ti substrate. Clear TiC peaks are observed for the substrates exposed at angles 0°, 10° and 15°. The intensities of the TiC peaks at 20° are very low in comparison with the other Ti peaks. For example, the intensity of the first TiC peak ($2\theta = 35.98°$) at 20° is almost seven times less than that at 0°. The sharpening of the diffraction peaks is observed with decreasing angular positions. The size of TiC crystallites was about 30–50 nm, as calculated from the width of the XRD peaks at 0° using the Scherrer equation. The XRD pattern of ion exposed Ti substrates at different angular positions using the copper anode (figure 2(*b*)) exhibits no characteristic peaks of TiC. In this case we observed Cu peaks on the XRD pattern of ion exposed Ti substrates at 0°. The observation of the Cu peaks at $2\theta = 43.25°$ and 50.41°, respectively, is due to the emission and deposition of copper from the electrode material.

The changes in the surface morphology due to the ion irradiation on Ti substrates at different angular positions using graphite and copper anodes are shown in figures 3(*a*) and (*b*), respectively. A surface growth of different structures of sub-micrometre size is clearly seen in the SEM micrographs. It is interesting to note that different surface morphologies appear with the change in the angular positions in two different anode materials. In the case of the graphite anode, at 0° the surface appears almost smooth with few cracks on it, whereas at 10°, 15° and 20° worm-like structures are observed on the substrates. A close observation of the SEM micrographs reveals the growth of worm-like structures with decreasing angular positions, from 20° to 10°. At 15° we observed dense arrays of these nanostructures coming out from the substrate surface, whereas at 10° these structures are curved. The growth of carbon nanostructures was reported by Gao *et al* [27], using thermal chemical vapour deposition of ethylene on iron-coated titanium substrates combined with a solid state reaction. They have reported the formation of dense and uniform arrays of well-aligned carbon nanotubes on titanium substrates filled with single crystals of TiC. They observed that when the tube diameter was smaller, the carbon nanotubes were curved and only partially filled with TiC. Though the presence of TiC is observed in the XRD spectra, in our case it is difficult to identify from the SEM micrographs whether the nanostructures are titanium carbide filled carbon nanotubes or simply carbon nanostructures. But it is important to note here that the AES results to be described below show that the top layer of the ion exposed substrate is carbon rich. In the case of the copper

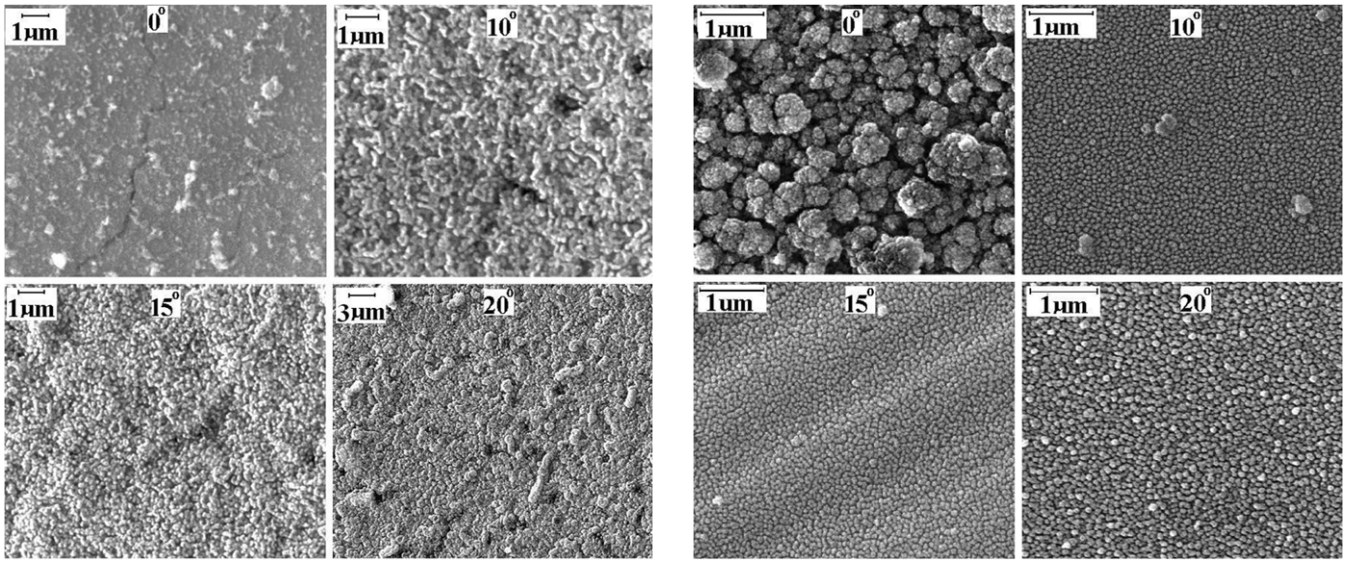

Figure 3. SEM micrograph of ion exposed Ti substrates at angular positions 0°, 10°, 15° and 20° in (*a*) graphite and (*b*) copper anodes.

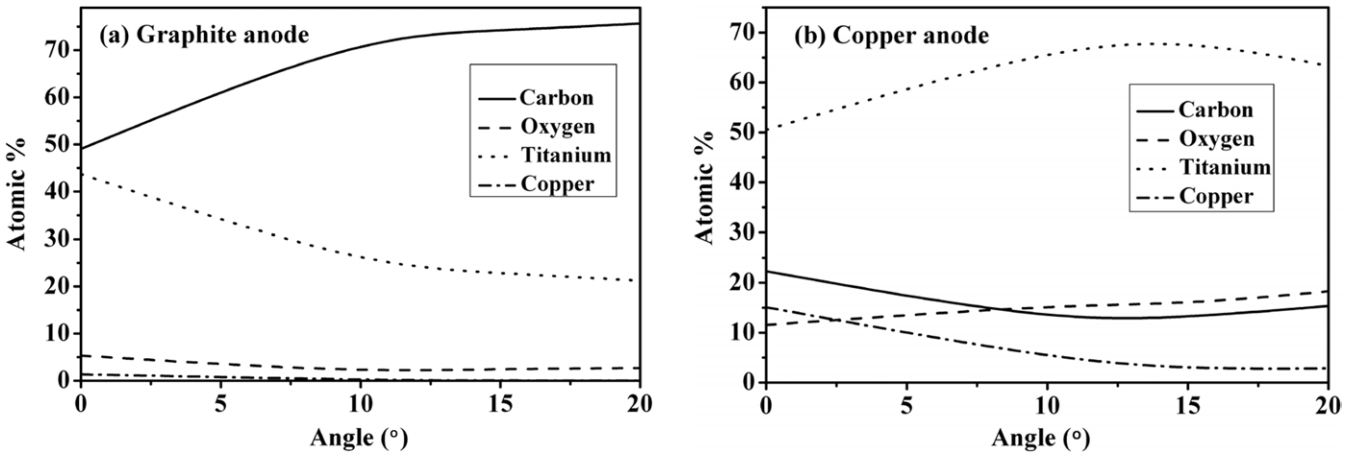

Figure 4. Atomic percentages of different elements on the ion exposed Ti substrates at different angular positions using (*a*) graphite and (*b*) copper anodes, drawn from EDX spectra.

anode, the surface morphologies at different angular positions are almost identical and the surfaces are covered by sub-micrometre size granules (figure 3(*b*)). At 0° it can be noticed that in some places many small sized grains have aggregated to form bigger sized grains. The grain size as well as the aggregation of smaller sized grains are found to decrease with the increase in angular positions.

The EDX spectra of the ion exposed Ti substrate shows the existence of carbon and oxygen along with copper, irrespective of the anode material. These elements are observed in all the substrates exposed at different angular positions. Figures 4(*a*) and (*b*) show the variation in atomic percentage of different constituents with the angular positions in the graphite and copper anodes, respectively. Comparing the atomic percentages of different constituents we observed that in the case of the graphite anode the carbon percentage on the substrate is almost twice that of the copper anode, whereas the copper percentage on the substrate is less than half. In the case of the copper anode, the peak of carbon arises only due to the dissociation of the methane plasma and the copper is eroded from the electrodes, whereas in the case of the graphite anode, carbon appears not only due to the dissociation of the methane plasma but also from the anode material. The small amount of copper seen in the latter case is eroded from the electrode materials, where a part of the anode was copper. The presence of oxygen can be ascribed to the absorption of oxygen by the unexposed Ti substrate before ion irradiation and also to the high Ti reactivity with residual water in the vacuum chamber. During the deposition process some of the oxygen content on/near the surface layer is removed due either to ion sputtering or to surface hydrogenation. In the case of the graphite anode, the relative intensity ratio of the carbon-to-titanium peak in the EDX spectrum increases with the increase in the angular positions. This indicates the increase in the thickness of the deposited layer with the increase in the angular positions. It is also observed that with the increasing angular positions the carbon content increases while the oxygen content decreases. But these tendencies are

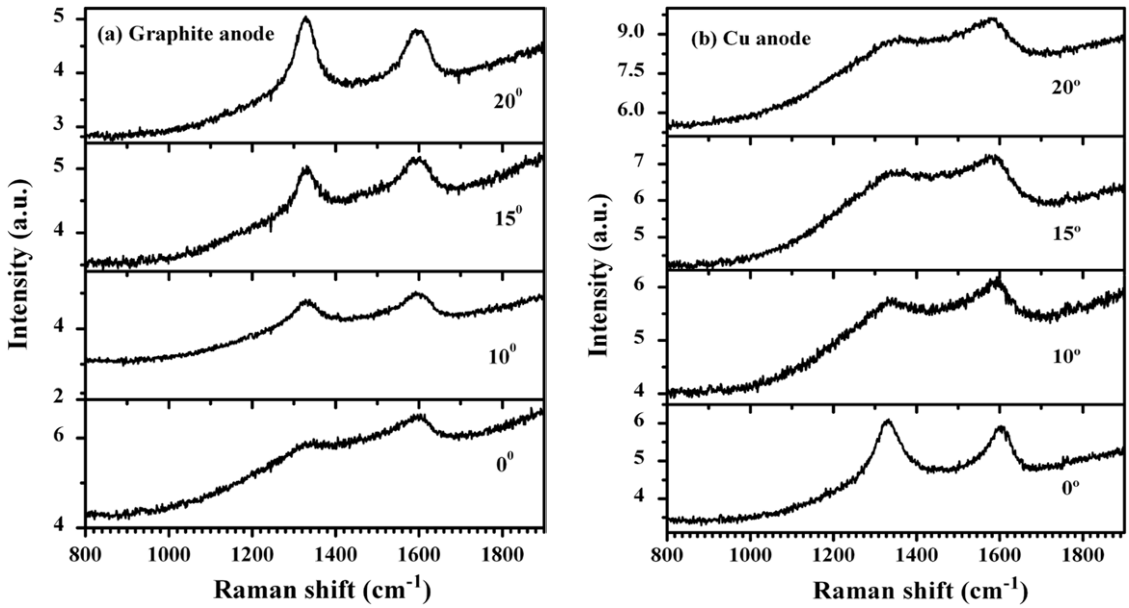

Figure 5. Raman spectra of ion exposed Ti substrate at angular positions 0°, 10°, 15° and 20° in (*a*) graphite and (*b*) copper anodes.

not seen in the case of the copper anode. In this case, the carbon content decreases and oxygen content increases with increasing angular positions. The thickness of the deposited layer decreases with the increase in the angular positions. The decrease or increase in atomic percentage of oxygen with increasing angular positions observed in the EDS spectra is probably due to the resulting variations in the thickness of the deposited layer on the substrate surface, keeping in mind that most of the oxygen is absorbed by the substrate before ion irradiation and resides near the interface. The EDX technique uses an electron beam to excite the elements present in a substrate, where the EDX detector collects and analyses the resultant x-rays from the substrate to give the atomic percentages of the elements. In addition to the incoming beam energy, the penetration of the electron beam depends on the nature and thickness of the deposited layer to be analysed. When the thickness of the deposited layer increases, the electron beam barely reaches the substrate surface or interface area to give the exact atomic percentages of the elements present.

The Raman spectra of ion exposed Ti substrate at different angular positions with graphite and copper anodes are shown in figures 5(*a*) and (*b*), respectively. Distinct Raman peaks are observed at around 1350 cm^{-1} and 1585 cm^{-1}, which correspond to the first order D and G bands, respectively. These D and G bands, with varying intensity, position and width, dominate the Raman spectra of nanocrystalline and amorphous carbons [28–31]. The G band or the graphite band appears due to the lattice vibration of sp^2 bonded carbon atoms. If the size of the graphite domains decreases, a low frequency modulation corresponding to the disordered zone of graphite gives rise to the D band or disorder-induced band. The broadening of the D and G bands relates to disorder within the carbon structures [28, 29]. The results presented are the average over three spectra recorded at different positions on the substrates. In the case of the graphite anode, it is observed that with increasing angular positions the full width at half maximum (FWHM) of the D and G peaks decreases almost linearly. D decreases from 340 cm^{-1} at 0° to 150 at 20° whereas G decreases from 130 cm^{-1} at 0° to 100 at 20°. The intensities of the Raman peaks increase with increasing angular positions, which, in turn, indicates the increase in the thickness of the carbon layer [28] and it is in good agreement with our AES results to be described below. The sharper G and D peaks with increasing angular positions also indicate the growth of nanocrystalline graphite. The ratio $I(D)/I(G)$ is lower at 10° and 15° and is higher at 0°. Lower $I(D)/I(G)$ ratios and sharper D and G peaks are known to be an indication of highly aligned and spatially ordered carbon nanostructures [30]. In addition, the higher $I(D)/I(G)$ ratio can be associated with a decline in structural order [31]. In the case of the copper anode we observed an increasing FWHM of the D peak with increasing angular positions. The ratio $I(D)/I(G)$ is minimum at 10° and 15°. The intensities of the Raman peaks decrease with increasing angular positions indicating the decrease in the thickness of the carbon layer. In one of our previous studies on ion beam anisotropy in PF, we have characterized the emission of high Z ions from the PF plasma [24]. These high Z ions have larger Larmor radius and thus they are deviated from the axial direction. These off axis copper ions cause substantial radiation damage and sputtering of the film that has already been deposited up to the previous focus shot (PF discharge). This is probably the reason for the decreasing thickness observed with increasing angular positions.

The elemental depth concentration profiles and the interface structure were investigated by the AES, only in the case of the graphite anode, as the XRD results indicate the formation of TiC. Figures 6(*a*)–(*d*) show the depth profile spectra of the ion exposed Ti substrates at different angular positions. It is observed that the substrate surfaces are composed of Ti, C and O elements. Each spectrum was taken three times under identical experimental conditions in order

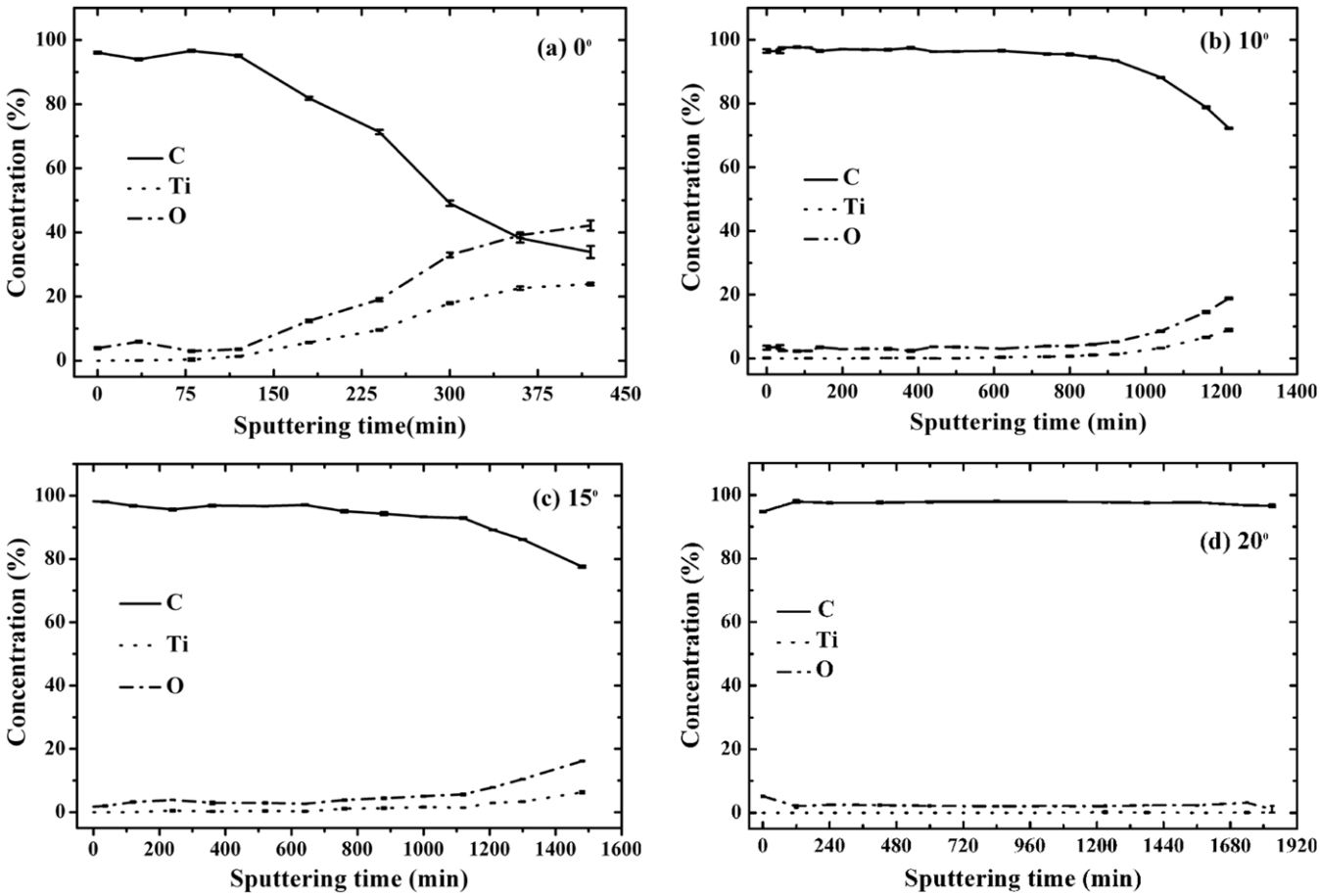

Figure 6. AES depth profile spectra of the ion exposed Ti substrates at different angular positions in graphite anode (*a*) 0° (*b*) 10° (*c*) 15° and (*d*) 20°.

to calculate systematic errors. The raw data were five points-smoothed and differentiated to measure Auger peak-to-peak height (APPH) for carbon (C KLL), titanium (Ti LMM and LMV) and oxygen (O KLL). Relative sensitivity factors were used to calculate the concentration for each element [32]. In the case of the substrate exposed at 0° we observed a gradual change in C, O and Ti concentrations with sputtering time. At a sputtering time of around 120 min the C concentration starts to decrease whereas the O and Ti concentrations increase. The increasing rate of O is similar to the decreasing rate of C, but different from the increasing rate of Ti. On the other hand, the C concentration of the substrates exposed at 10°, 15° and 20° starts to decrease at sputtering times of around 800 min, 1000 min and 1500 min, respectively. This indicates the increase in the thickness of the deposited layer with increasing angular positions. The results of the profiles show that the top layer is C rich. In all the cases, we observed the increase in O concentration near the interface, giving evidence that the oxygen is mainly absorbed by the unexposed Ti substrate before ion irradiation. The dissimilar rates of increase of O and Ti are also observed in the latter cases, which indicates that not only TiO_x, but also TiC are present at the interface; otherwise, the carbon layer would act as a filter and the absolute value of the TiO_x and C rates would be equal. Figures 7(*a*) and (*b*) show C (KLL) spectra and Ti (LMM and LMV) spectra, respectively, of the substrates exposed at 0° for different sputtering times. In the case of the C KLL Auger peak, a shift is observed (from 272 to 277 eV) after 120 min sputtering, indicating different chemical states in that depth [33]. This kind of shift in the C Auger peak towards higher energy is responsible for the compound formation at the interface [34, 35]. The shift is also observed for the substrates exposed at 10°, 15° and 20°. As shown in figure 7(*b*), before sputtering no Ti peak was observed, but after 80 min sputtering, two weak Ti peaks at 384 and 416 eV were measured. These Ti peaks are shifted to 386 and 419 eV after 420 min sputtering. The shift between the substrate and the interface indicates the possibilities of formation of different chemical states, such as TiO_x and TiC. Although the interpretation of this spectrum is very complex, a recent work suggests that due to the surviving oxygen, titanium oxide compound could be formed [36]. Considering the formation of TiO_x, TiC and C gradient layers on the substrate surface, we have calculated the thicknesses of the exposed substrates using Monte Carlo simulation of electron trajectory in solids [37]. Table 1 shows the thickness of the different layers formed on the substrates placed at different angular positions. A thicker TiC layer is observed on the substrate placed at 0° where the C layer is thinner. On the other hand, a thinner TiC layer is found on the substrate placed at off axis where the C layer is thicker. The thickness of the TiO_x layer is relatively thin at all angular positions.

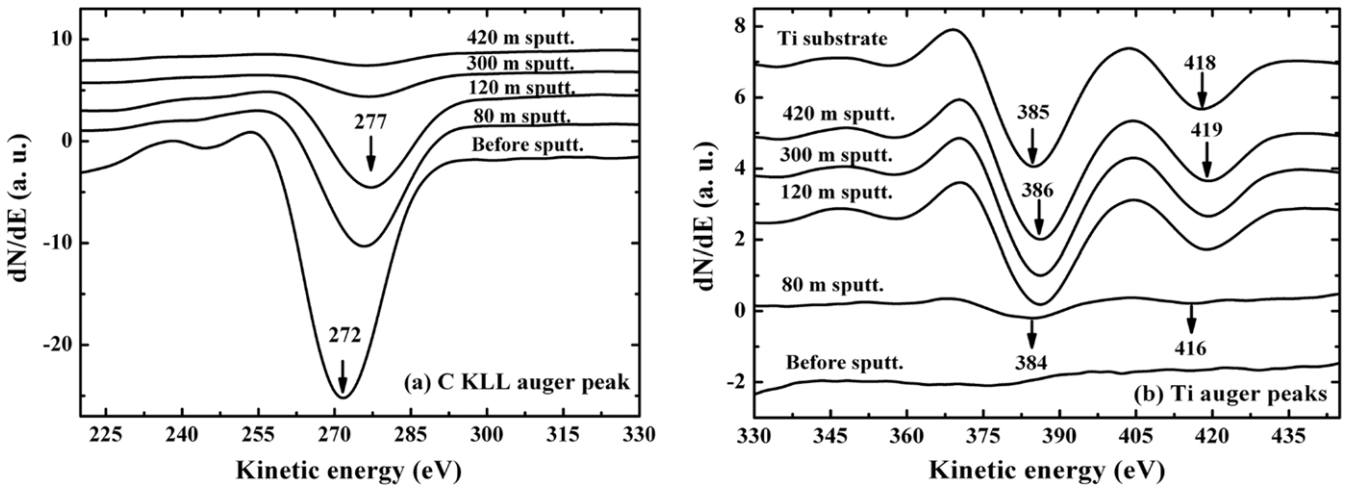

Figure 7. Auger peak positions at different sputtering time for (*a*) C (KLL) and (*b*) Ti (LMM and LMV) spectra. Substrates exposed at 0° using graphite anode.

Table 1. Thickness of the layers formed on the substrates placed at different angular positions in graphite anode.

Substrates	C (nm)	TiC (nm)	TiO_x (nm)	Total thickness (nm)
0°	139	500	29	668
10°	868	75	14.0	957.0
15°	950	55	16.0	1021.0
20°	1110	25	19.0	1154.0

The dependence of angular positions, including charge states, energy spectrum and flux of the ion beams emitted from this PF device has been characterized earlier using the time of flight (TOF) technique, with an array of miniature Faraday caps [16, 24]. A detailed explanation on the analysis procedure for the identification of different peaks in the ion signal has been given in [16]. TOF measurements of the ion emission at different angular positions operating in methane showed that the main ion beam components correspond to H^+, C^{+5} and C^{+4} irrespective of the angular direction with respect to the PF axis [24]. In addition to that, we have also observed emission of metal vapours from the electrode material. The estimated maximum ion energies for H^+, C^{+4} and C^{+5} are in the range 150–300 keV, 300–500 keV and 700–1000 keV, respectively, whereas their fluxes ($\sim 10^{22}$ ions m^{-2} s^{-1}) are maximum for the energy ranges 15–40 keV, 50–100 keV and 100–300 keV, respectively. The angular distribution of hydrogen and carbon ions shows a highly anisotropic character. The fluxes of carbon ions are found to be maximum off axis whereas their energies are maximum on axis. The maximum ion emission was observed at an angle of 15° with respect to the anode axis. It is known that in PF, the ion beam interacts with the substrate surface in two ways [38, 39]. On the one hand, the ion dose is adequate to change the physical properties of the substrate surface and on the other hand, the energy delivered by the ion beam raises the surface temperature to a high value, without noticeable changes in the bulk temperature, which can promote the diffusion of the ions on the substrate surface. In addition to that, plasma bubble or the electrode vapour, generated by the disruption of the plasma column is also responsible for the growth of structures [25]. Computer simulations of the thermal evolution of solid targets under PF ion beam irradiation have been performed using realistic ion beam fluxes measured in a similar PF device [40]. The results indicate that transient heating of the target takes place at heating slopes and speeds as high as 3600 K μm^{-1} and 40 K ns^{-1}, respectively, with the maximum temperature high enough for melting and evaporation of the surface layers. Although the underlying process and growth mechanisms in our case are complex, it is anticipated that all the kinetic energies of the penetrated ion species at the substrate surface are converted into thermal energy. Just after the ion penetration the vapours ejected from the anode material reach the substrate surface. As a result, the surface is heated up to very high temperatures in a short time, which is immediately followed by rapid melting and re-solidification. This fast heating can also play a thermal annealing role in subsequent shots. During this process the collision cascades lead to intermixing of the materials at the interface. The high thermal gradient, high heating and cooling rates can result in the formation of the observed growth structures on our substrates. The XRD and AES results indicate the formation of a TiC layer, only in the case of the graphite anode. We have irradiated the substrates by 50 PF discharges. During the first few discharges the ion beams followed by the anode vapour penetrate into the titanium substrates and interact to form a TiC interface. After a few discharges the substrate surface saturates and starts depositing carbon over the TiC layer. Although the ion beam consists of hydrogen and carbon ions, it is speculated that the formation of a TiC layer is mainly responsible for the carbon vapours ejected from the anode tip. This is the reason why we have not observed the formation of TiC in the case of the copper anode. The anode vapour mainly emitted towards the PF axis thereby produces a thicker TiC layer at 0° compared with the other angular positions. At the PF axis the highly energetic ions from the following PF discharge, besides helping in the growth process, can also cause substantial radiation damage and sputtering of the film that has already been deposited up to

the previous PF discharge. This is probably the reason why we observed the minimum C layer on the substrate placed at 0°, where the ion energy is found to be maximum. On the other hand, at off axis we observed thicker C layers, because of the low energy-high flux ions.

4. Conclusions

We have investigated the effect of high energy ion beam irradiation on Ti substrates at room temperature using a low energy PF device operating in methane gas. A combination of XRD, SEM, EDX, RS and AES techniques has provided a reasonably comprehensive characterization of the physical and chemical properties of the nanocomposite layers deposited in the graphite and copper anodes. The ion irradiated surface morphologies with two different anode materials, graphite and copper, are different. In the case of the graphite anode, we observed the growth of nanowires whereas in the case of the copper anode the surfaces were covered by sub-micrometre size granules. The composite layer deposited using the graphite anode was composed of a nano-TiC phase and an amorphous C phase whereas only an amorphous C phase was observed in the case of the copper anode. The thickness of the TiC layer was maximum at 0° whereas at other angular positions we observed a thin layer of TiC near the interface and an increasing amount of carbon as the surface was approached. The formation of a TiC layer is the consequence of ion and anode vapour implantation on a Ti substrate at room temperature without external substrate heating and post-annealing at high temperature. Nanocomposite layers demonstrate superior mechanical properties, but optimization and further progress are reliant upon adequate characterization and a good understanding of the nanostructures formed. Further work is required to improve the understanding of the formation of carbon nanostructures in PF.

Acknowledgments

This work has been funded by the FONDECYT grant 11060343/7080136, and partially by the FONDECYT grant 1071058. MECESUP UCH 0205 is acknowledged for Auger electron spectroscopy. The technical assistance of Marcela Soto, Manuel Pino, Dirk De Jong and David Alvarez is highly appreciated.

References

[1] Baker M A 2007 *Surf. Coat. Technol.* **201** 6105
[2] Robertson J 2002 *Mater. Sci. Eng.* R **37** 129
[3] Pauleau Y and Thiery F 2004 *Surf. Coat. Technol.* **180–181** 313
[4] Galvan D, Pei Y T and Hosson J M 2006 *Surf. Coat. Technol.* **201** 590
[5] Hu Y, Li L, Cai X, Chen Q and Chu P K 2007 *Diamond Relat. Mater.* **16** 181
[6] Lin J, Moore J J, Mishra B, Pinkas M and Sproul W D 2008 *Thin Solid Films* **517** 1131
[7] Liepack H, Bartsch K, Arnold B, Bauer H D, Liu X, Knupfer M and Leonhardt A 2004 *Diamond Relat. Mater.* **13** 106
[8] Wang Y, Zhang X, Wu X, Zhang H and Zhang X 2008 *Appl. Surf. Sci.* **254** 5085
[9] Yang B, Huang Z H, Gao H T, Fan X J and Fu D J 2007 *Surf. Coat. Technol.* **201** 6808
[10] Martínez-Martínez D, López-Cartes C, Fernández A and Sánchez-López J C 2009 *Thin Solid Films* **517** 1662
[11] Voevodin A A, Capano M A, Laube S J P, Donley M S and Zabinski J S 1997 *Thin Solid Films* **298** 107
[12] Soto G 2004 *Appl. Surf. Sci.* **230** 254
[13] Luthin J, Plank H, Roth J and Linsmeier Ch 2001 *Nucl. Instrum. Methods. Phys. Res.* B **182** 218
[14] Tong H H, Monteiro O R and Brown I G 2001 *Surf. Coat. Technol.* **136** 211
[15] Shum P W, Zhou Z F and Li K Y 2004 *Wear* **256** 362
[16] Bhuyan H, Chuaqui H, Favre M, Mitchell I and Wyndham E 2005 *J. Phys. D: Appl. Phys.* **38** 1164
[17] Mather J W 1971 *Methods of Experimental Physics* vol 9B ed H Griem and R H Lovberg (New York: Academic) p 187
[18] Kelly H, Lepone A, Marquez A, Lamas D and Oviedo C 1996 *Plasma Sources Sci. Technol* **5** 704
[19] Nayak B B, Acharya B S, Mohanty S R, Borthakur T K and Bhuyan H 2001 *Surf. Coat. Technol.* **145** 8
[20] Bhuyan H, Favre M, Valderrama E, Avaria G, Chuaqui H, Mitchell I, Wyndham E, Saavedra R and Paulraj M 2007 *J. Phys. D: Appl. Phys.* **40** 127
[21] Zhang T, Thomas Gan K S, Lee P, Ramanujan R V and Rawat R S 2006 *J. Phys. D: Appl. Phys.* **39** 2212
[22] Rawat R S, Lee P, White T, Ying L and Lee S 2001 *Surf. Coat. Technol.* **138** 159
[23] Rawat R S, Aggarwal V, Hassan M, Lee P, Springham S V, Tan T L and Lee S 2008 *Appl. Surf. Sci.* **255** 2932
[24] Bhuyan H, Favre M, Valderrama E, Chuaqui H and Wyndham E 2006 *J. Phys. D: Appl. Phys.* **39** 3596
[25] Lepone A, Kelly H, Lamas D and Marquez A 1999 *Appl. Surf. Sci.* **143** 124
[26] The International Centre for Diffraction Data® http://www.icdd.com/
[27] Gao Y, Liu J, Shi M, Elder S H and Virden J W 1999 *Appl. Phys. Lett.* **74** 3642
[28] Knight D S and White W B 1989 *J. Mater. Res.* **4** 385
[29] Sattel S, Robertson J and Ehrhardt H 1997 *J. Appl. Phys.* **82** 4566
[30] Chhowalla M, Teo K B K, Ducati C, Rupesinghe N L, Amaratunga G A J, Ferrari A C, Roy D, Robertson J and Milne W I 2001 *J. Appl. Phys.* **90** 5308
[31] Abbas G, Papakonstantinou P, Iyer G R S, Kirkman I W and Chen L C 2007 *Phys. Rev.* B **75** 195429
[32] Davis L E, MacDonald N C, Palmberg P W, Riach G E and Weber R E 1976 *Handbook of Auger Electron Spectroscopy* (Eden Prairie, MN: Perkin-Elmer Corporation) p 13
[33] Haas T W, Grant J T and Dooley G J 1972 *J. Appl. Phys.* **43** 1853
[34] Swart H C, Jonker A J, Claassens C H, Chen R, Venter L A, Ramoshebe P, Wurth E, Terblans J J and Roos W D 2003 *Appl. Surf. Sci.* **205** 231
[35] Maline M, Ducarroir M, Teyssandier F, Hillel R, Berjoan R, Loo F J J and Wakelkamp W 1993 *Surf. Sci.* **286** 82
[36] Zou Y, Wang L W and Huang N K 2007 *Thin Solid Films* **515** 5524
[37] Drouin D, Réal C A, Joly D, Tastet X, Aimez V and Gauvin R 2007 *Scanning* **29** 92
[38] Feugeas J, Lionch E C, de Gonzalez C O and Galambos G 1988 *J. Appl. Phys.* **64** 2648
[39] Feugeas J N, Sanchez G, Gonzalez C O, Hermida J D and Scordia G 1994 *Rad. Eff. Defects Solids* **128** 267
[40] Sanchez G and Feugeas J 1997 *J. Phys. D: Appl. Phys.* **30** 927